Optoelectronic properties of calcium cobalt oxide misfit nanotubes

Luc Lajaunie,[1,2,3,a)] Ashwin Ramasubramaniam,[4,a),b)] Leela S. Panchakarla,[5] and Raul Arenal[1,6,b)]

[1]Laboratorio de Microscopías Avanzadas, Instituto de Nanociencia de Aragón, Universidad de Zaragoza, 50018 Zaragoza, Spain
[2]Departamento de Ciencia de los Materiales e Ingeniería Metalúrgica y Química Inorgánica, Facultad de Ciencias, Universidad de Cádiz, Campus Río San Pedro S/N, Puerto Real 11510, Cádiz, Spain
[3]Instituto Universitario de Investigación de Microscopía Electrónica y Materiales (IMEYMAT), Facultad de Ciencias, Universidad de Cádiz, Campus Río San Pedro S/N, Puerto Real 11510, Cádiz, Spain
[4]Department of Mechanical and Industrial Engineering, University of Massachusetts Amherst, Amherst, Massachusetts 01003, USA
[5]Department of Chemistry, Indian Institute of Technology Bombay, Mumbai 400076, India
[6]ARAID Foundation, 50018 Zaragoza, Spain

We report on the optoelectronic properties of a recently discovered nanotubular phase of misfit-layered calcium cobalt oxide, $CaCoO_2$–CoO_2. Individual nanotubes are investigated by spatially resolved electron energy-loss spectroscopy experiments performed in a transmission electron microscope, and complementary first-principles, time-dependent hybrid density-functional theory calculations are performed to elucidate the electronic structure and optical spectra. We find that the band gap is independent of the geometry of the nanotubes, and experimental and calculated results independently confirm an optical gap of 1.9–2.1 eV for the $CaCoO_2$–CoO_2 nanotubes. The time-dependent hybrid density-functional theory calculations also suggest the existence of strongly bound intralayer excitons (up to 0.5 eV binding energy), which could allow for optoelectronic applications of these nanotubes at near-infrared to visible (~1.5–2 eV) wavelengths. *Published by AIP Publishing.* https://doi.org/10.1063/1.5043544

Misfit layered compounds (MLCs) are materials that are composed of stacks of chemically and structurally dissimilar layers with incommensurate lattice parameters.[1–3] While the existence of MLCs derived from layered oxides and chalcogenides has been known for several decades, these materials are attracting renewed interest for high-performance thermoelectrics based on their unusual ability to function simultaneously as electron crystals and phonon glasses.[4] MLCs also offer unique opportunities to study physics in reduced dimensions both within 2D sheets of the layered structure as well as in 1D nanotubular forms that have been synthesized more recently.[5–10] In particular, misfit-oxide based nanotubes (NT), the most recent additions to the MLC family, have been shown to display hitherto unknown sub-stoichiometric oxide phases and are semiconducting unlike the metallic bulk phase.[7,8] Thus, these 1D misfit oxides hold promise for applications in the fields of optoelectronics and thermoelectrics, and are also of fundamental interest by virtue of being strongly-correlated low-dimensional systems.

Recently, we synthesized and characterized a new nanotubular misfit-oxide phase, $CaCoO_2$–CoO_2, from the well-known bulk phase of calcium cobaltite, Ca_2CoO_3–CoO_2.[7] The nanotubular phase is formed upon selective leaching of CaO from one side of the Ca_2CoO_3 layer within the bulk phase, which leads to a loss of inversion symmetry that in turn drives scrolling of the overall structure as a strain relaxation mechanism. Using a combination of high-resolution

scanning transmission electron microscopy (HR-STEM), electron energy-loss spectroscopy (EELS), and density functional theory (DFT) calculations, we showed that the nanotubes consist of alternate layers of hexagonal CoO_2 and $CaCoO_2$ along the *c*-axis [Fig. 1(a)]. DFT calculations also predicted the $CaCoO_2$–CoO_2 phase to be semiconducting (~1.2 eV band gap). The optoelectronic properties of $CaCoO_2$–CoO_2 have, however, not yet been explored and are the focus of this letter.
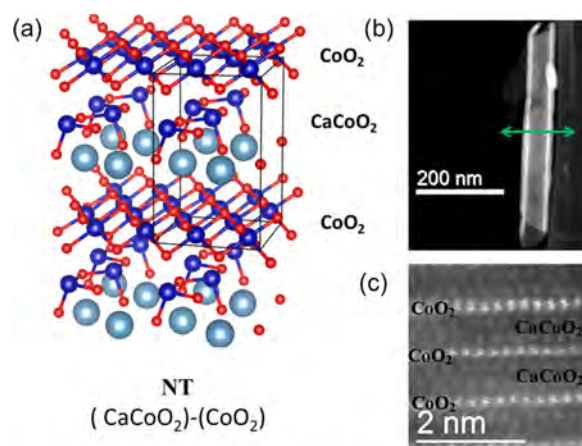

FIG. 1. (a) Structural model (unit cell indicated with solid lines) of misfit-layered $CaCoO_2$-CoO_2 phase of calcium cobaltite; cyan, blue, and red spheres indicate Ca, Co, and O atoms, respectively. (b) STEM-high-angle annular dark field (HAADF) image of one the NTs studied in this work. The green arrow highlights the direction of the EELS scan line. Only the central region of the NT was used to extract the band-gap. (c) HR-STEM HAADF micrograph taken at the edge of one NT.

[a)]L. Lajaunie and A. Ramasubramaniam contributed equally to this work.
[b)]Authors to whom correspondence should be addressed: ashwin@engin.umass.edu and arenal@unizar.es

We used spatially-resolved EELS (SR-EELS) measurements within a transmission electron microscope fitted with a monochromator to determine the low-energy response of the nanotubes and to extract the value of the band-gap.[11,12] This approach allows us to selectively probe individual nanotubes from a mix of nanosheets, nanoscrolls (nanosheets rolled up into spiral structures), and nanowires that are the typical products of our synthetic methods.[7] Complementing these measurements, we also report EELS spectra simulations from time-dependent hybrid density functional theory calculations that are capable of capturing important electron–hole interactions in these low-dimensional systems. The time-dependent calculations—unlike the independent-particle (IP) approach—show good agreement with EELS measurements, and the two sets of independent results confirm an optical gap in the range of 1.9–2.1 eV for $CaCoO_2$–CoO_2 nanotubes. Interestingly, the time-dependent calculations also suggest the existence of strongly bound, intralayer excitons (up to 0.5 eV binding energy), which renders these nanotubes of interest for optoelectronics in the near-infrared.

Aberration-corrected high-resolution scanning transmission electron microscopy (HR-STEM) experiments were performed using a FEI Titan Low-Base microscope operated at 80 kV and equipped with a CESCOR Cs probe corrector, an ultra-bright X-FEG electron source and a monochromator. HR-STEM imaging was performed by using high-angle annular dark field (HAADF) detector. SR-EELS scan-line experiments were performed with the monochromator excited to determine the optical properties of the nanotubes. The EELS scan lines were performed perpendicular to the long axis of the nanotubes [Fig. 1(b)] and, to avoid edge effects, only the central regions of the nanotubes were used to extract the band-gap. Five different nanotubes were analyzed to check the reproducibility of the results. The crystalline nature of the nanotubes and the stacking of the two sub-systems are clearly highlighted by the HR-STEM HAADF images [Fig. 1(c)]. The energy resolution was 180 meV with a dispersion of 0.02 eV per pixel, and the acquisition time was about 0.3 s per pixel (total acquisition time ∼2 min). The data were then aligned on the energy scale by using the zero-loss peaks (ZLP) as reference and denoised by using the principal component analysis (PCA) routines of the Hyperspy software.[13] The Richardson-Lucy deconvolution algorithm was employed to improve the energy resolution (see Fig. S1 of the supplementary material).[11,12,14] For this purpose, the point-spread function was determined by using an aligned ZLP spectrum recorded far away from the nanotube. The number of iterations was limited to one to avoid the introduction of artifacts. After this process the energy resolution was improved to 160 meV. The ZLP was subtracted from the dataset by using the aligned ZLP taken in the vacuum after deconvolution (Fig. S2). This procedure has been successfully employed previously to determine the band gap of other oxide-based nanostructures.[15] The band gap was determined via the linear fitting method which yields reliable results for monochromated spectra.[11,16]

The Vienna *Ab Initio* Simulation Package (VASP) was employed for DFT and hybrid DFT electronic structure calculations.[17,18] The calculation procedures at the DFT+U level have been described in our previous work,[7] which we

refer the reader to for complete details. Here, we provide additional details as relevant to the hybrid-DFT calculations. Starting from DFT+U-optimized atomic structures and wavefunctions, we performed spin-polarized calculations using the Heyd-Scuseria-Ernzerhof (HSE) functional with a kinetic energy cutoff of 525 eV, a Γ-centered $8 \times 8 \times 4$ k-point mesh for Brillouin zone sampling, and 256 bands per spin channel. The electronic bandstructure was calculated along the high-symmetry directions via Wannier interpolation.[19] The converged HSE wavefunctions were employed in a spin-polarized time-dependent HSE (TDHSE) calculation with 32 occupied bands and 16 virtual bands for electron-hole interactions, which provides a sufficiently large energy window to capture accurately (vertical) optical transitions up to ∼3 eV. The local part of the DFT exchange-correlation kernel was also included in the time-dependent calculations. Due to the significant computational cost of spin-polarized HSE and TDHSE calculations for this 20-atom supercell, we used a reduced $2 \times 2 \times 1$ q-point grid for calculating the Fock exchange potential. As an independent check, we compared frequency-dependent absorption spectra from HSE and single-shot GW calculations that were found to be in reasonable agreement at low energies (Fig. S3).

The electronic structure of the $CaCoO_2$-CoO_2 phase has been reported in our previous work at the DFT+U level.[7] Figure 2 displays the electronic bandstructure and density of states calculated with the HSE functional. In general, the HSE and DFT+U calculations are in qualitative agreement with both approaches predicting a semiconducting, ferrimagnetic (6 μ_B per unit cell) ground state. The majority spin carriers localizes primarily on the $CaCoO_2$ layer, whereas the minority carriers localizes on the CoO_2 layers. The conduction band edge is dominated by states from the CoO_2 layer whereas the valence band edge has contributions from both the $CaCoO_2$ and CoO_2 layers. In particular, the CoO_2 states at the conduction band edge, visible as a sharp resonance in the density of states, arise from localized states on the Co atoms and form a nearly flat, dispersionless band. Quantitatively, the most significant difference between HSE
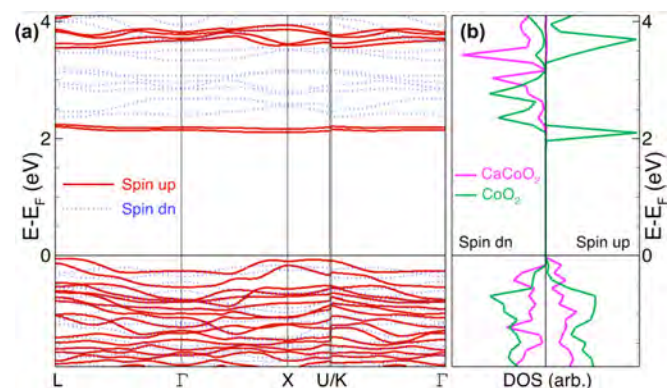

FIG. 2. (a) Electronic bandstructure and (b) layer-wise density of states of $CaCoO_2$-CoO_2 calculated with the HSE hybrid-DFT functional. The unit cell is ferrimagnetic with a net magnetization of 6 μ_B, and indirect band gaps of ∼2.1 eV and ∼2.5 eV in the spin-up and spin-down channels, respectively. The conduction band edge is dominated by states from the CoO_2 layer whereas the valence band edge has contributions from both the $CaCoO_2$ and CoO_2 layers.
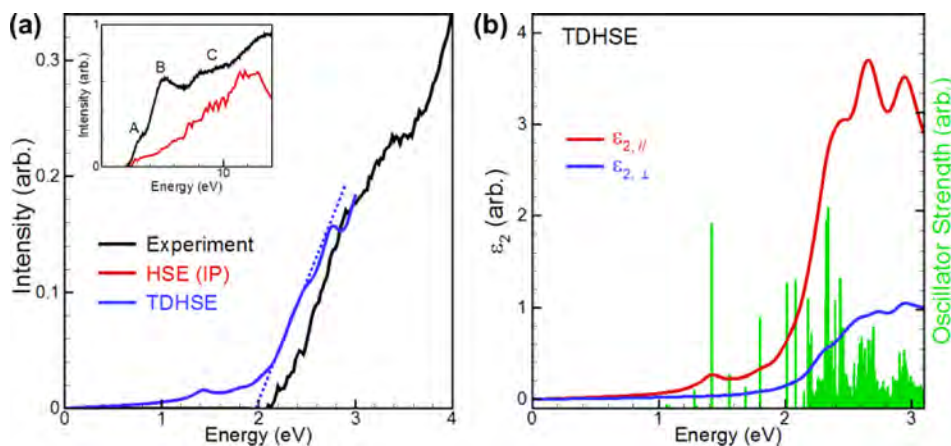
FIG. 3. (a) Comparison of low-energy experimental and TDHSE EELS spectra for $CaCoO_2$-CoO_2; the inset shows the experimental and HSE spectra for a wider range of energies. (b) In-plane and out-of-plane components of the TDHSE frequency-dependent absorption spectrum, $\varepsilon_2(\omega)$. Vertical green bars represent the cumulative oscillator strengths for optical transitions at different energies.

and DFT+U calculations is that the HSE functional predicts electronic band gaps of approximately 2.1 eV and 2.5 eV for the majority and minority spin channels, respectively, and these gaps are now appreciably larger than the corresponding DFT+U values of 1.2 eV and 1.3 eV.[7] As we show below, the HSE estimate for the band gap is more reasonable when compared with experiments as opposed to DFT+U results that employ the commonly used empirical Hubbard correction of U-J = 4 eV for strongly-correlated Co d-electrons.[4,20]

In the inset of Fig. 3(a), we display a typical experimental EELS spectrum extracted at the center of a nanotube. The low-loss energy spectrum display three main features, labeled A, B, and C, situated at 3.4, 5.2, and 8.8 eV, respectively. All the probed nanotubes show a similar EELS response (Fig. S4) although some slight differences in the intensity of the C feature can be observed. The origin of these differences at higher-energy is not clear at the moment, but comparison between spectra taken at the center and at the edge of the nanotubes suggests that it comes from different intermixing of the in-plane and out-of-plane components (Fig. S5). Nevertheless, all nanotubes show similar absorption onset indicating that the band gap is independent of their geometry. The value of the experimental band gap, extracted from the EELS spectra, is 2.15 ± 0.15 eV. For comparison, the fundamental gap obtained from the HSE functional is 2.1 eV and 2.5 eV for the majority and minority spins, respectively. However, the HSE fundamental gap does not correspond directly to the measured gap and furthermore, as seen from the inset of Fig. 3(a), the independent-particle (IP) HSE EELS spectrum differs even at the qualitative level from the measured EELS spectrum. Therefore, to make direct connection with the EELS measurements, we calculated the frequency-dependent dielectric tensor within the time-dependent (TDHSE) framework. As the TDHSE calculation is extremely computationally expensive, we restrict attention to an energy window of 0–3 eV for optical excitations, which is sufficient to identify important features related to the absorption onset and low-energy excitonic features. It is immediately apparent that the TDHSE EELS spectrum is in significantly better agreement with experiment [Fig. 3(a)], reproducing the slope of the EELS spectrum past 2 eV quite satisfactorily, albeit with a slightly earlier onset (~0.1 eV).

A closer inspection of the TDHSE EELS spectrum shows a slight shoulder around 1.5 eV and, as seen from the

absorption spectrum in Fig. 3(b), this shoulder arises exclusively from the in-plane component of the absorption spectrum. In general, we observe a few optical transitions with appreciable oscillator strengths within the 1–2 eV window that is suggestive of strongly bound in-plane excitons (~0.5 eV binding energy) within the misfit-layered structure. As the HSE functional suffers from a lack of exact exchange in the long-range, the TDHSE calculations do not offer definitive proof of the presence of bound excitons in our system.[21,22] Prior work does show though that TDHSE typically produces reasonable absorption spectra for medium gap semiconductors[23] and hence, our results furnish a useful starting point for future investigations of the quantitative details of exciton binding energies via more rigorous, albeit computationally expensive, many-body theory. The sharper onset of absorption in the measured EELS spectra relative to calculations, could also be a consequence of the breakdown of magnetic order at room temperature in which case one could expect the flat, "defect-like," majority-spin CoO_2 states [Fig. 2(a)] to acquire some dispersion and merge into the conduction band; this would in turn led to more continuum-like absorption. Future work will examine these issues in more detail.

In summary, we have studied the optoelectronic properties of $CaCoO_2$–CoO_2 misfit nanotubes by a combination of monochromated EELS experiments and time-dependent hybrid density-functional theory calculations. The band gap is independent of the geometry of the nanotubes and both measurements and electronic structure calculations confirm optical gaps in the range of 1.9–2.1 eV. Our calculations also suggest the presence of strongly bound intralayer excitons that could allow for optoelectronic applications of these nanotubes at near-infrared to visible wavelengths.

See supplementary material for experimental spectrum after PCA denoising and Richardson-Lucy deconvolution; experimental spectrum after ZLP subtraction; comparison of HSE and GW spectra, comparison of the low-loss EELS spectra measured at the center of five different nanotubes; and comparison between spectra taken at the center and at the edge of one nanotube.

[1]G. Wiegers and A. Meerschaut, *Materials Science Forum* (Trans Tech Publications, Switzerland, 1992), pp. 101–172.

[2]J. Rouxel, A. Meerschaut, and G. Wiegers, J. Alloys Compd. **229**, 144 (1995).

[3]G. Wiegers, Prog. Solid State Chem. **24**, 1 (1996).

[4]A. Rébola, R. Klie, P. Zapol, and S. Öğüt, Phys. Rev. B **85**, 155132 (2012).

[5]G. Radovsky, R. Popovitz-Biro, M. Staiger, K. Gartsman, C. Thomsen, T. Lorenz, G. Seifert, and R. Tenne, Angew. Chem., Int. Ed. **50**, 12316 (2011).

[6]L. S. Panchakarla, L. Lajaunie, R. Tenne, and R. Arenal, J. Phys. Chem. C **120**, 15600 (2016).

[7]L. S. Panchakarla, L. Lajaunie, A. Ramasubramaniam, R. Arenal, and R. Tenne, ACS Nano **10**, 6248 (2016).

[8]L. S. Panchakarla, L. Lajaunie, A. Ramasubramaniam, R. Arenal, and R. Tenne, Chem. Mater. **28**, 9150 (2016).

[9]L. Lajaunie, G. Radovsky, R. Tenne, and R. Arenal, Inorg. Chem. **57**, 747 (2018).

[10]B. Višić, L. S. Panchakarla, and R. Tenne, J. Am. Chem. Soc. **139**, 12865 (2017).

[11]R. Arenal, O. Stéphan, M. Kociak, D. Taverna, A. Loiseau, and C. Colliex, Phys. Rev. Lett. **95**, 127601 (2005).

[12]R. Arenal, O. Stéphan, M. Kociak, D. Taverna, A. Loiseau, and C. Colliex, Microsc. Microanal. **14**, 274 (2008).

[13]F. de la Peña, P. Burdet, T. Ostasevicius, M. Sarahan, M. Nord, V. T. F. J. Taillon, A. Eljarrat, S. Mazzucco, G. Donval, L. F. Zagonel, M. Walls, and I. Iyengar, HyperSpy: Multidimensional Data Analysis Toolbox (2015).

[14]A. Gloter, A. Douiri, M. Tence, and C. Colliex, Ultramicroscopy **96**, 385 (2003).

[15]E. D. Hanson, L. Lajaunie, S. Hao, B. D. Myers, F. Shi, A. A. Murthy, C. Wolverton, R. Arenal, and V. P. Dravid, Adv. Funct. Mater. **27**, 1605380 (2017).

[16]J. Park, S. Heo, J.-G. Chung, H. Kim, H. Lee, K. Kim, and G.-S. Park, Ultramicroscopy **109**, 1183 (2009).

[17]G. Kresse and J. Furthmuller, Phys. Rev. B **54**, 11169 (1996).

[18]G. Kresse and D. Joubert, Phys. Rev. B **59**, 1758 (1999).

[19]A. A. Mostofi, J. R. Yates, G. Pizzi, Y.-S. Lee, I. Souza, D. Vanderbilt, and N. Marzari, Comput. Phys. Commun. **185**, 2309 (2014).

[20]A. Rébola, R. F. Klie, P. Zapol, and S. Öğüt, Appl. Phys. Lett. **104**, 251910 (2014).

[21]Z. Yang and C. A. Ullrich, Phys. Rev. B **87**, 195204 (2013).

[22]Z. Yang, F. Sottile, and C. A. Ullrich, Phys. Rev. B **92**, 035202 (2015).

[23]J. Paier, M. Marsman, and G. Kresse, Phys. Rev. B **78**, 121201 (2008).